Journal of the European Ceramic Society 19 (1999) 2487–2501

PII: S0955-2219(99)00125-9
0955-2219/99/$ - see front matter

Microstructural Stability and Mechanical Properties of Directionally Solidified Alumina/YAG Eutectic Monofilaments

L. E. Matson [a]* and N. Hecht [b]

[a]Materials and Manufacturing Directorate, Air Force Research Laboratory, USAF/AFRL/MLLN, WPAFB, OH 45433, USA
[b]University of Dayton, Dayton, Ohio 45469, USA

Abstract

Fiber strength retention and creep currently limit the use of polycrystalline oxide fibers in ceramic matrix composites making it necessary to develop single crystal fibers. Two-phase alumina/YAG single crystal structures in the form of monofilaments show that the room temperature tensile strength increases according to the inverse square root of the microstructure size. Therefore, microstructure stability will play a significant role in determining the 'use temperature' of these fibers along with its creep resistance. In this work, the effects of temperature on microstructural stability and the creep behavior of directionally solidified alumina/YAG eutectic monofilaments were studied. Microstructural stability experiments were conducted in air from 1200 to 1500°C and creep tests at temperatures of 1400 to 1700°C. Inherent microstructure stability was found to be very good, however, extraneous impurity-induced heterogeneous coarsening was significant above 1400°C. The creep strength of monofilaments with aligned microstructures were superior to ones with low aspect ratio morphologies. Mechanisms for microstructural coarsening and creep behavior are discussed. © *1999 Elsevier Science Ltd. All rights reserved.*

Keywords: Al_2O_3, coarsening, creep, fibers, monofilaments, YAG.

1 Introduction

Oxide based fibers are regarded as the most desirable reinforcing material for ceramic matrix composites (CMCs) because of their inherent thermochemical stability in air.[1–5] Polycrystalline fibers are limited to a maximum useful temperature of between 1000 and 1200°C by fiber strength degradation and creep.[6,7] Rapid strength loss is due to grain growth while high creep rates are due to diffusional creep mechanisms, both phenomena are the consequence of grain boundaries. Single crystal fibers show superior creep resistance because the elimination of grain boundaries forces microstructural changes to occur through bulk and surface diffusional processes.[8–15] However, single crystal fibers are limited by a low fracture toughness (K_c) and strength degradation at moderate temperatures caused by flaws which undergo slow crack growth.[10,11,16–21]

In the hopes of overcoming the shortcomings of single crystal fibers, two-phase single crystals structures have been explored. Bulk eutectics show better K_c values than single crystals, but their creep resistance is limited by deformation and decohesion at misaligned colony boundaries.[22–24] Eutectic monofilaments have been fabricated using single crystal melt processes of edge-defined film-fed growth (EFG)[25–30] and laser heated float zoning (LHFZ).[31–33] Process control during directional solidification has resulted in either the colony boundaries being completely eliminated or aligned with the stress axis of the fiber. In this study, directionally solidified alumina/YAG eutectic [DS-AYE] monofilaments were selected because the CTE mismatch is low and the solid solubilities of constituent elements is very limited. Both properties are essential for thermal mechanical and microstructural stability.

Statistically designed growth experiment on DS-AYE monofilament using the edge-defined film-fed growth method (EFG) has been conducted at UES Inc.[34] and Saphikon Inc.[35]

Each study concluded.

(a) The fiber pull rate was the dominant processing parameter for increasing the steepness

*To whom correspondence should be addressed.

of the thermal gradient during solidification, hence, reducing the microstructural scale (as measured in the transverse section) in the monofilament.

(b) The phase alignment and its aspect ratio (as measure in the fiber growth direction) was increased when the pull rate was increased and a planar solidification front was maintained.

(c) It was anticipated that a reduction in fiber diameter would also reduce the phase size and result in an increase in strength, similar to what is seen in single crystal growth.[36,37] However, in this fiber system only minimal increase was noted by both vendors.

(d) The 'figure of merit property' in both studies was the room temperature (RT) tensile strength. It was concluded in both studies that the finer the transverse phase size the greater the RT tensile strength.

Figure 1 shows a plot of selected room temperature strengths of DS-AYE materials as a function of phase size from several investigations (including fiber and bulk processed eutectic melts) along with an empirical fit as predicted by the Hall-Petch type relationship. These data suggest that the RT tensile strength is proportional to the inverse square of the phase size (a Hall Petch type relationship) similar to what is observed in polycrystalline ceramics. Thus, the critical processing flaw size must be constrained to within an alumina/YAG phase dimension in the as-grown fibers. Strength retention at high temperatures or after long term anneals should be predictable by the homogeneous coarsening behavior. However, in this system severe strength degradation problems have recently been reported after long term anneals[32,38–41] and attributed to a discontinuous coarsening mechanism.[42,43] Strength limiting defects appear on the fiber surface as abnormal coarsened areas which are distributed heterogeneously. The first part of this work will focus on a systematic heat treatment study coupled with SEM, EDX, and TEM analysis to clarify the coarsening mechanisms in the system and its effects on strength will be discussed. The second part of this work will focus on the creep behavior of the system and how phase alignment effect creep. Methods to obtain the reliable steady state creep data will be discussed.

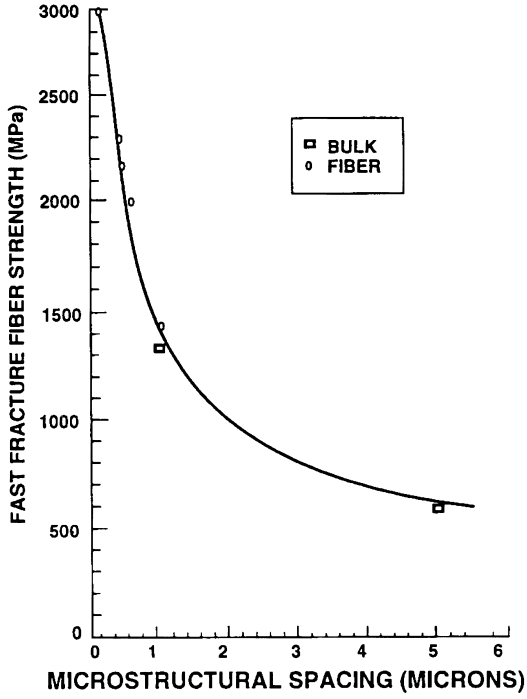

Figure 1. RT fast fracture tensile strength of DS-AYE. Curve fit with an inverse square root function.

2 Experimental Procedures

2.1 Fiber processing and characterization

DS-AYE monofilaments grown using the EFG process were obtained from UES Inc. (Dayton, OH) and Saphikon Inc. (Milford, NH). TEM Selected Area Diffraction analysis showed that both monofilaments had the same orientation relationship (OR) between phases $(0001)_A//(111)_Y$, $(1010)_A//(011)_Y$, $[1120]_A//[211]_Y$ but each had distinctly different microstructures. Monofilaments from the UES statistically designed growth experiment were used in this study and contained a Chinese script morphology throughout.[22–29] The backscattered SEM micrographs of the longitudinal and transverse section of an as-fabricated UES fiber is shown in Fig. 2(a). The microstructure consists of a fine lamellar structure containing YAG single crystals (bright phase) distributed in a matrix of single crystal Alumina (dark phase). The volume fraction of phases was determined digitally to be approximately (55% YAG). This value agrees with what is predicted by the phase diagram.[44–49] For creep testing, the UES monofilament selected had a large microstructural scale and a low aspect ratio. The average thickness of the YAG phase (as measured in the transverse section) of approximately 0·5 μm, while the average length of the YAG phase with respect to the fiber tensile axis was approximately 5 μm.

Most monofilaments produced by Saphikon using the EFG process were similar in microstructure to the UES fiber. One exception was a lot of monofilament which had a very unique microstructure consisting of a single colony containing rod/plate type eutectic morphology surrounded by a casing of a uniform Chinese script morphology [fiber designation (YAE-1, machine 28, die 29)], [Fig. 2(b)]. The rod/plate colony occupied about 50 vol% of the fiber and contained extremely fine

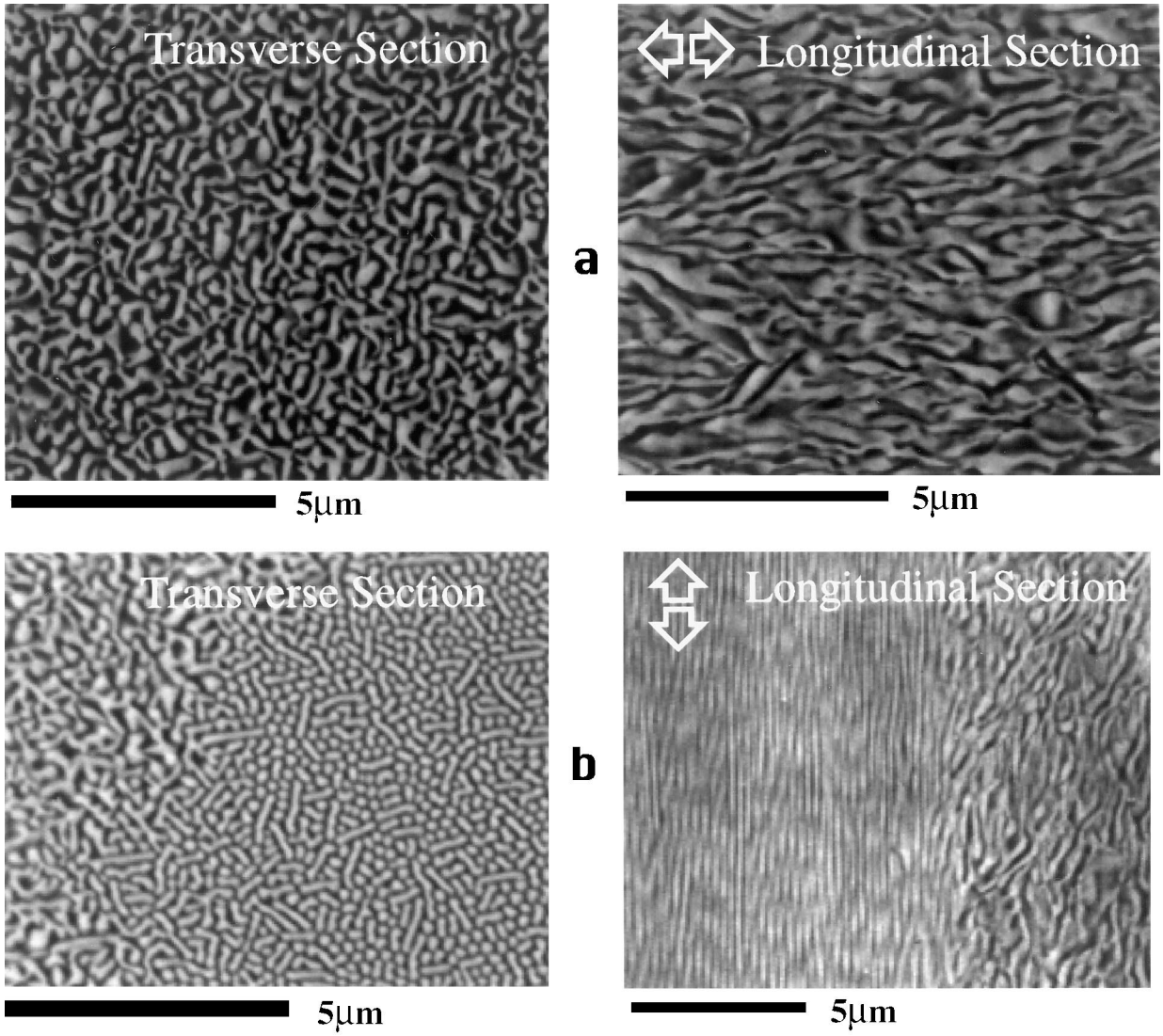

Fig. 2. SEM backscattered micrographs of AYE monofilaments from 2 vendors. The fiber growth direction is indicated with arrows. (a) Uniform Chinese script morphology from UES monofilament grown at 0·5 in min^{-1}. (b) Colony microstructure of the Saphikon monofilament (Chinese script morphology at the rim and continuous rod/plate lamella in the core).

phase sizes which were highly aligned. The YAG phase thickness was 0·15 μm and lengths of nearly infinity. While the Chinese script section at the fiber rim contained YAG phase thickness of 0·25 μm and lengths of approximately 5 μm. A detailed explanation for the growth conditions which lead to this unique colony microstructure is not clear at the present time. However, colony formation may be due to the melt being slightly hyper-eutectic in composition or that one phase took the lead in the solidification causing a non-uniform solidification front. In either case, the microstructure of this monofilament allowed for validation of the strength and creep hypotheses without the complication of different orientation relationships between the interpenetrating Alumina and YAG single crystal phases.

In both monofilaments the alignment of the microstructure with respect to the fiber axis was not always perfect but meandered about the axis of the fiber. This growth phenomena is also found in C-axis sapphire production.[18,19,50] The effect of processing variables on the meander was not studied in this experiment; in fact its occurrence was minimized by careful selection of the fibers being tested. In the creep experiments where 12 inch long fiber sections were needed the microstructure was characterized at both ends to assure good alignment and colony centering.

2.2 Microstructural stability

Anneals were performed in air using an 8 inch (20·32 cm) vertical sapphire tube furnace containing molybdenum disilicide elements which allowed for a 2 inch (5·08 cm) constant temperature zone. The sapphire tube had an opening of 1/4 inch (0·635 cm) diameter; which allowed for four monofilaments to be suspended in the furnace at a given time. The furnace was heated at a rate of 6°C min^{-1} to the desired exposure temperature and fibers were removed after 1, 10, 50, and 100 h exposures. Exposures were performed at temperatures ranging from 1200 to 1500°C in approximately 100°C

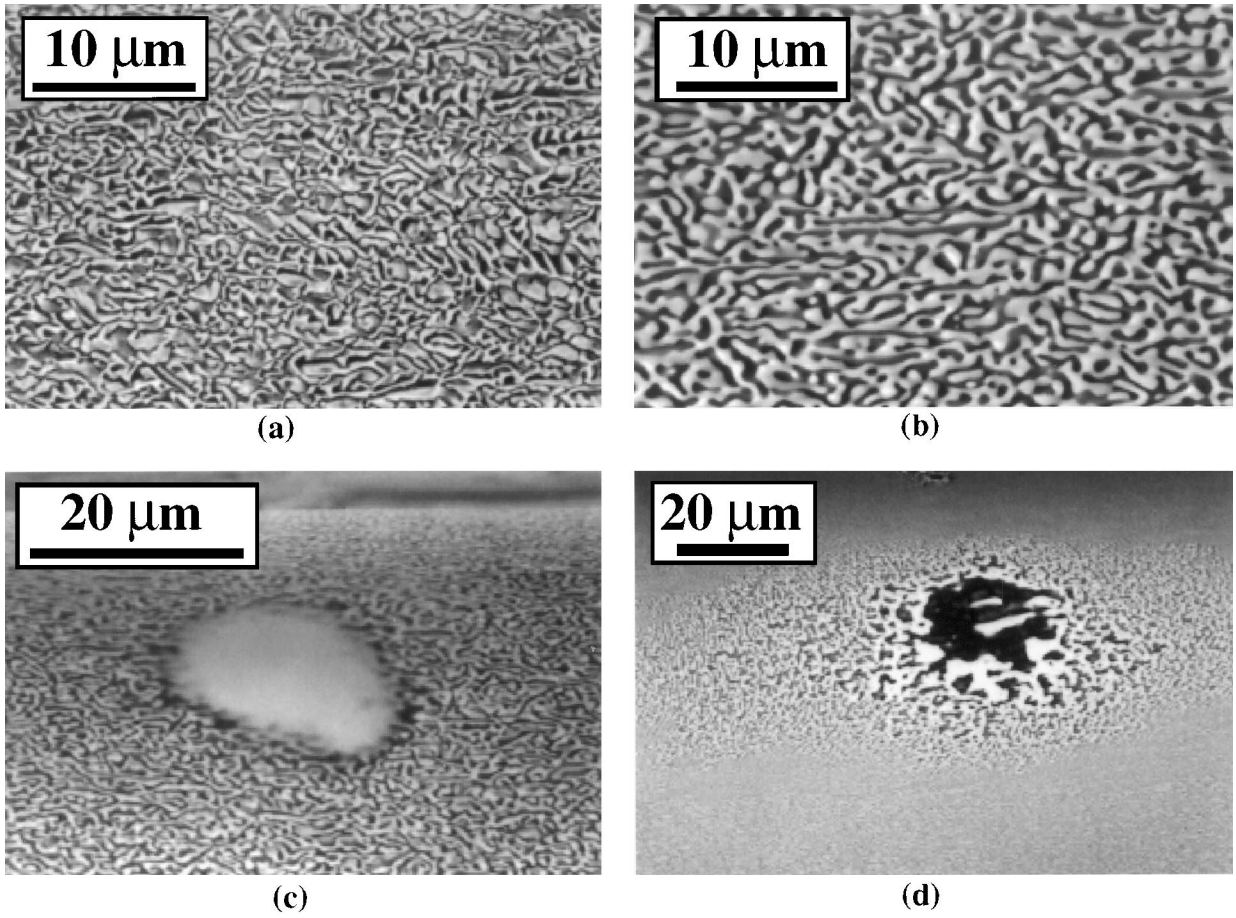

Fig. 3. SEM micrographs of fiber surface. (a) As received. UES monofilament grown at 0·5 in min^{-1}. (b) Homogeneous coarsening after annealing at 1500°C, 100 h in air. (c) Heterogeneous coarsening after short-term anneal at 1400°C, 10 h. (d) Heterogeneous coarsening after long-term anneal at 1400°C, 50 h.

increments. This furnace design was selected to assure no reaction of the furnace element environment with the monofilaments. Some monofilaments were intentionally allowed to collect dust in ambient conditions while others were cleaned and handled with scrupulous care.

The heat-treated fibers were mounted on a stainless steel ruler and carbon coated for evaluation in a Leica FEG 360 SEM equipped with a Noran (EDX) Spectrometer. Backscattered electron SEM micrographs of select fiber surfaces are shown in Fig. 3 to illustrate homogeneous and heterogeneous coarsening. The location of heterogeneous defects on the fiber surfaces were noted so that 'site specific' TEM foils could be prepared at a later date. The heat treated fibers were cut, mounted, and polished to yield longitudinal and transverse cross sections. These samples were evaluated in the SEM for phase volume fraction, size, shape, and alignment. 'Site specific' TEM thin foils were successfully prepared in a Philips SEM coupled with a FEI Focused Ion Beam (FIB) milling unit. TEM micrographs, crystallographic analysis using Selected Area Diffraction (SAD), and chemical analysis were performed using a Philips FEG 200 TEM equipped with a Noran (EDX) Spectrometer and a Gatan DigiPEELS unit.

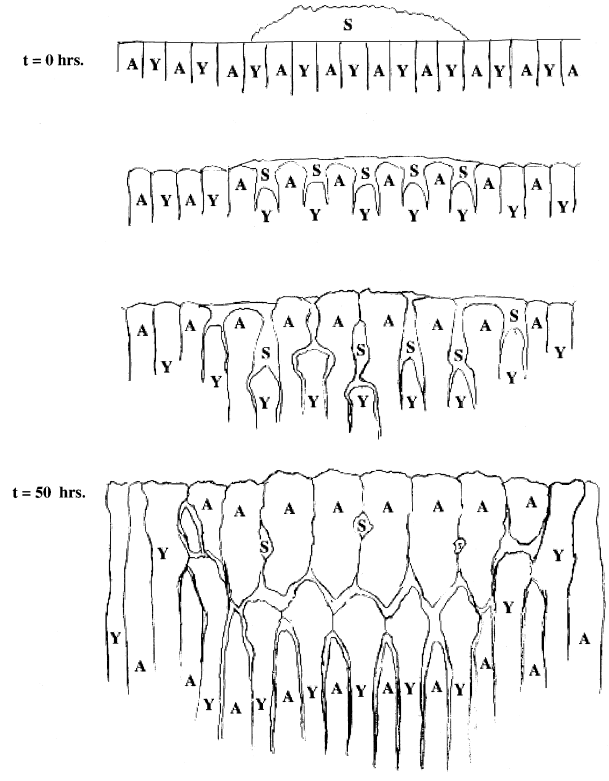

Fig. 4. Model of heterogeneous coarsening shown as a function of time.

2.3 Creep experiment

Cold grip-constant load tensile creep testing was conducted in air using a vertical sapphire tube furnace that contained an inductively coupled molybdenum susceptor. Details of the design are given by Sheehan.[11,13,51–53] This furnace has a hot zone of approximately 0·5 in (1·27 cm) at 1500°C as defined by a ±10°C span. Displacements were measured using a linear variable displacement transducer with the core rod attached between the end of the fiber and the weight. Argon was used to protect the molybdenum susceptor which resided between the OD of the 1/8 inch (3·175 mm) diameter sapphire tube and the ID of a 2 inches (5·08 cm) quartz tube. Each tube was approximately 8 inch in length. An atmosphere of room air was maintained around the monofilament in the ID of the sapphire tube. The furnace temperature was controlled by a thermocouple placed between the sapphire tube and the molybdenum susceptor. Furnace profiling was done prior to and after each test using both a (Pt-Rh) thermocouple as well as an Accufiber optical thermocouple. Creep test was terminated upon rupture or after 200 h of exposure. Creep tests were performed at loads from 100 to 500 MPa and temperatures from 1400 to 1700°C. Crept samples were mounted on a stainless steel ruler and the fiber surface were characterized in an SEM. Transverse and longitudinal sections were prepared from the gage section and characterized by transmitted polarized light, SEM, EDX, and TEM. One creep test per setup was used so as not to confuse the analysis.

3 Results and Discussion

3.1 Homogeneous coarsening and strength retention

The homogenous coarsening of the rod/plate morphology found in the Saphikon DS-AYE

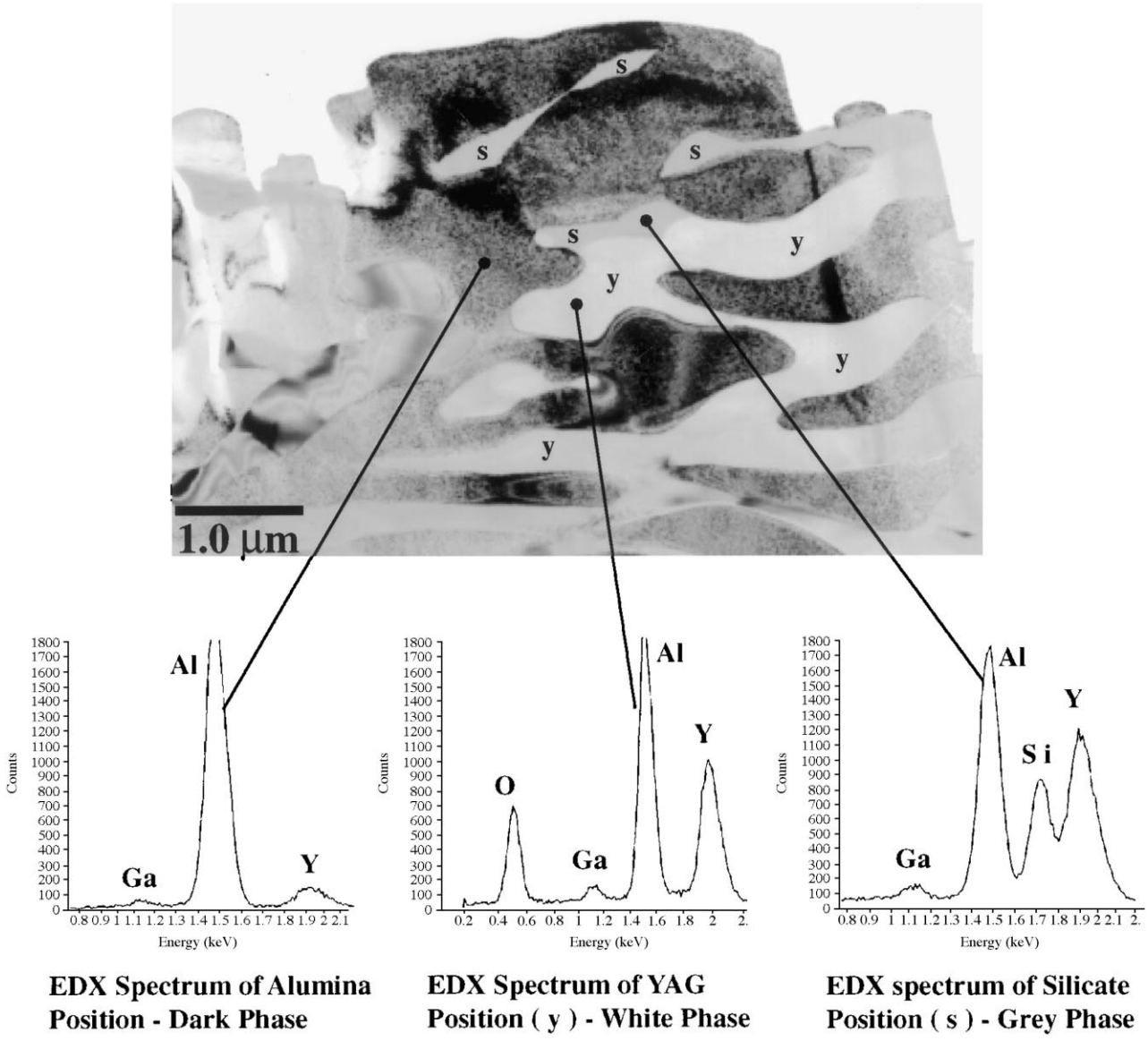

Fig. 5. TEM micrograph and EDX spectra of the surface defect found in Fig. 3(c). This is the initial stages of heterogeneous coarsening on an AYE-UES monofilament exposed for 10 h at 1500°C in air.

monofilament is very slow following ($t^{1/4}$) kinetics according to Yang.[41,54] His analysis was conducted using a classical rate theory approach most commonly used in grain growth analysis: $D^n - D_o^n = kt, k = Ae^{(-Q/RT)}$, where ($D$) is the instantaneous YAG phase thickness measured in the transverses cross section, (D_o) is the initial YAG phase thickness, (t) is the time, (n) is a constant, (k) is a kinetic constant (depending primarily on the temperature and the interfacial energy), (Q) is the activation energy, (T) is the absolute temperature, (R) is the gas constant, and (A) is an empirical constant. In polycrystalline, single phase grain growth, (A) is related to the frequency of atoms jumping across the grain boundary. In this two phase single crystal structure, it could be related to numerous phenomena, such as the frequency of kink formation at the interface boundary, the frequency of kink migration to the coarsening site: however, all of these phenomena are limited by diffusion of O, Al, or Y ions along the interphase boundary. According to Ardell 55,[55] the observed $t^{1/n}$ behavior where $n = 4$ is consistent with an interphase diffusion controlled mechanism.

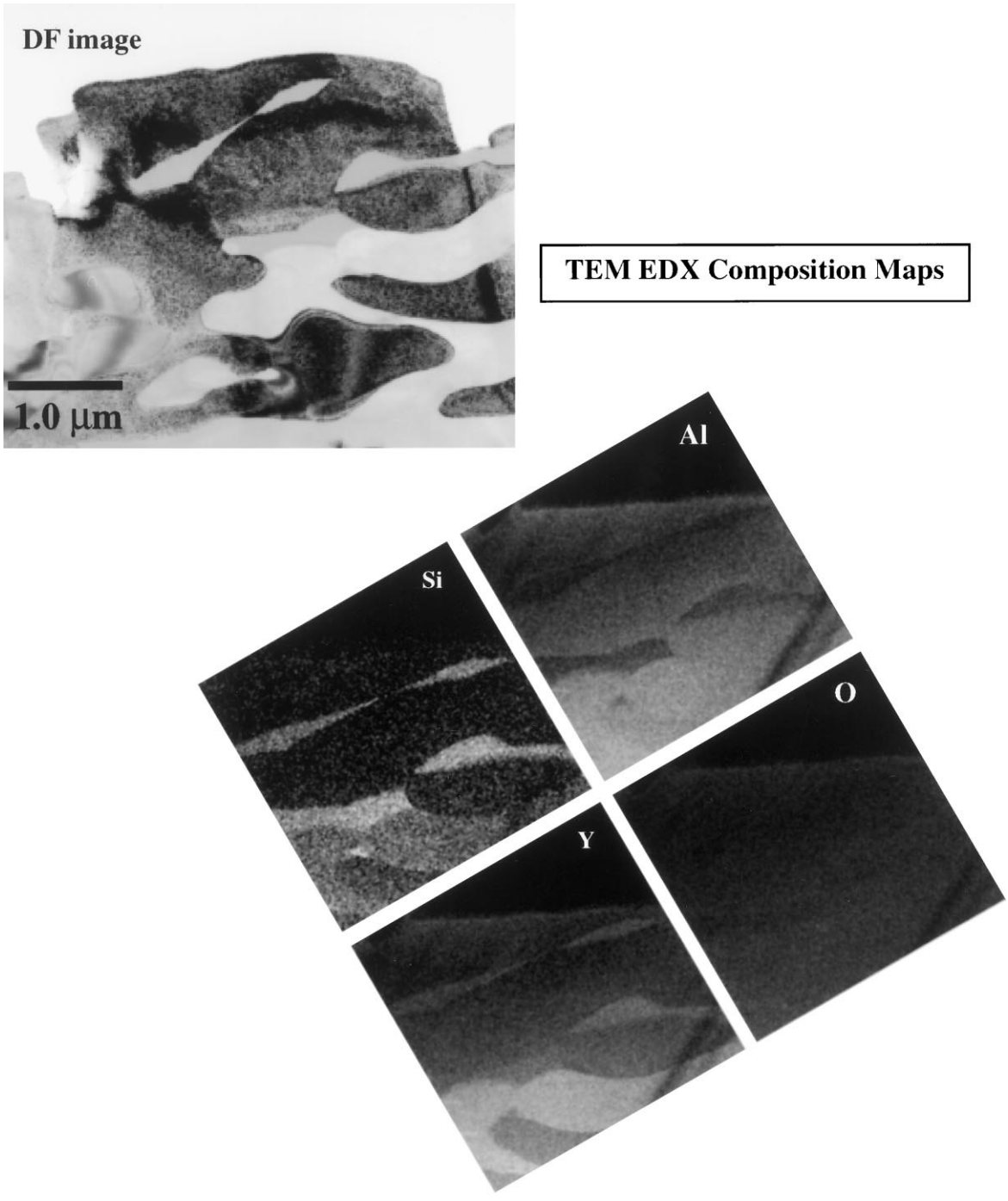

Fig. 6. EDX mapping of TEM micrograph from the surface defect found in Figs 3(c) and (5) showing the extent of reaction and the wetting of interphase boundaries by the silicate phase. This is the inital stages of heterogeneous coarsening on AYE-UES monofilament exposed for 10 h at 1500°C in air.

In Yang's work, the activation energy (Q) for the coarsening process was determined by plotting log $(D^4 - D_o^4)/t$ verses $1/T°K \times 10^{-4}$ and taking the slope. A value of $Q = 280$ kJ/°K-mol was obtained and it was suggested that the rate limiting step for the coarsening process was the bulk lattice diffusion of O^{2-} in YAG = 310 kJ/°K-mol.[56] However, in this system the oxygen sublattice only requires short range diffusion to meet the crystallographic constraints at the interface. Therefore, it is highly unlikely for O^{2-} ions to be the rate limiting species for homogeneous coarsening. More realistic would be the diffusion of Y^{3+} ions which is the heaviest and largest ion in both single crystal YAG and yttrium solid solutions in Sapphire. Unfortunately, the activation energy for grain boundary diffusion

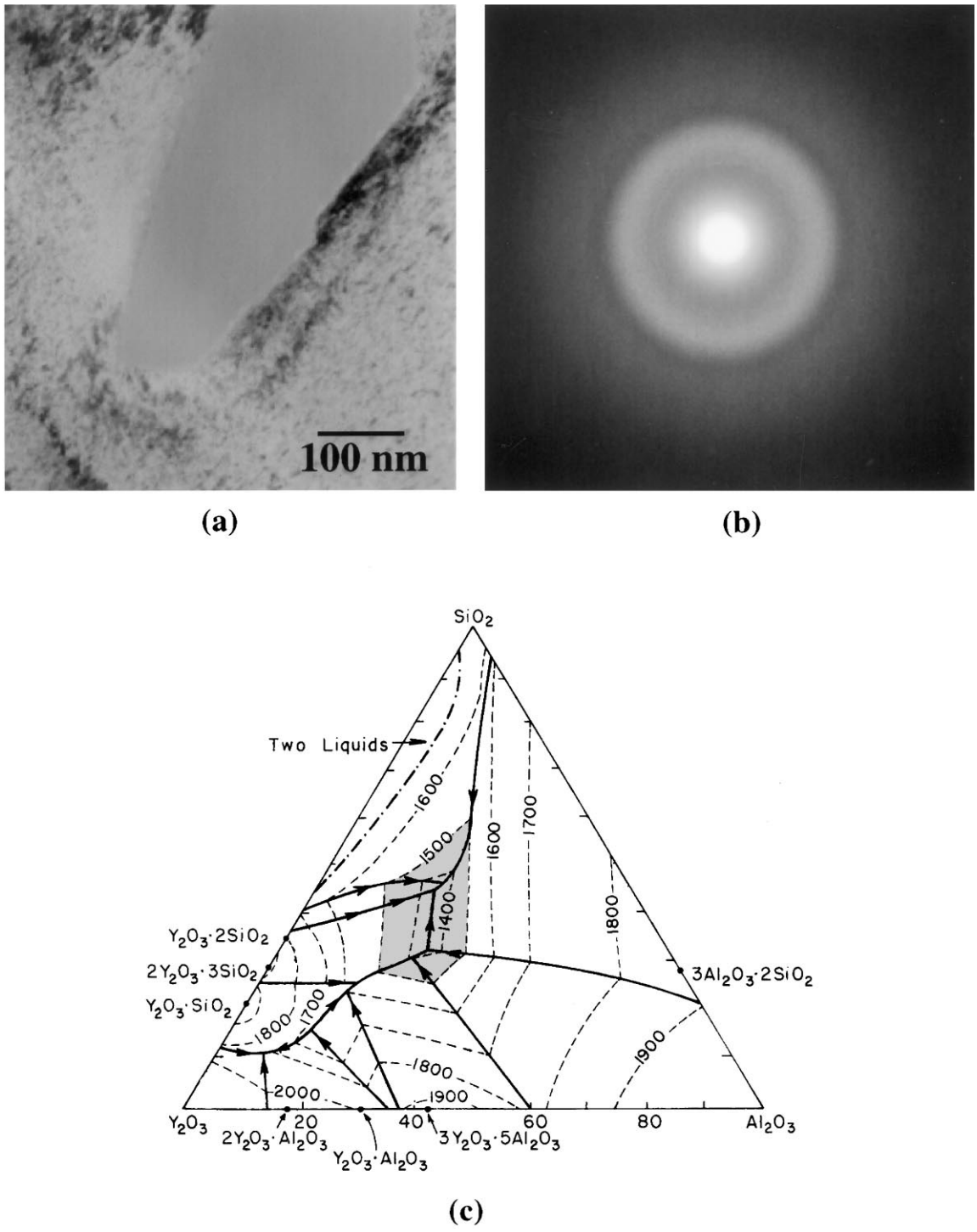

Fig. 7. TEM analysis of the surface defect found in Figs 3(c) and (5). (a) TEM BF micrograph showing large facets at the alumina–silicate interface. (b) TEM SAD pattern from the glassy silicate (grey) phase in (a). (c) Al_2O_3–Y_2O_3–SiO_2 ternary phase equilibrium diagram showing the liquidus surface. The shaded area shows the liquid compositions possible below 1500°C.[62]

of Y^{3+} ions in YAG has not been recorded in the literature. However, a reasonable estimate would be a value which is half that of Y^{3+} ions lattice diffusion in YAG. Parthasarathy[57] showed the activation energy for Nabarro–Herring creep [volume diffusion control creep] of polycrystalline YAG to be 587 kJ/°K-mol. Similarly, Hay[58] showed a $Q = 550$ kJ/°K-mol for the solid state reaction of sapphire + YAP → YAG. Each of these authors concluded that the rate limiting step was the lattice diffusion of the Y^{3+} ions. The value of 280 kJ/°K-mol reported by Yang is close to half of these reported activation energies for bulk lattice diffusion. Therefore, it is reasonable to suggest that the activation energy found for homogeneous coarsening by Yang is on the order that one would expect if interphase boundary diffusion of the Y^{3+} ions are rate limiting.

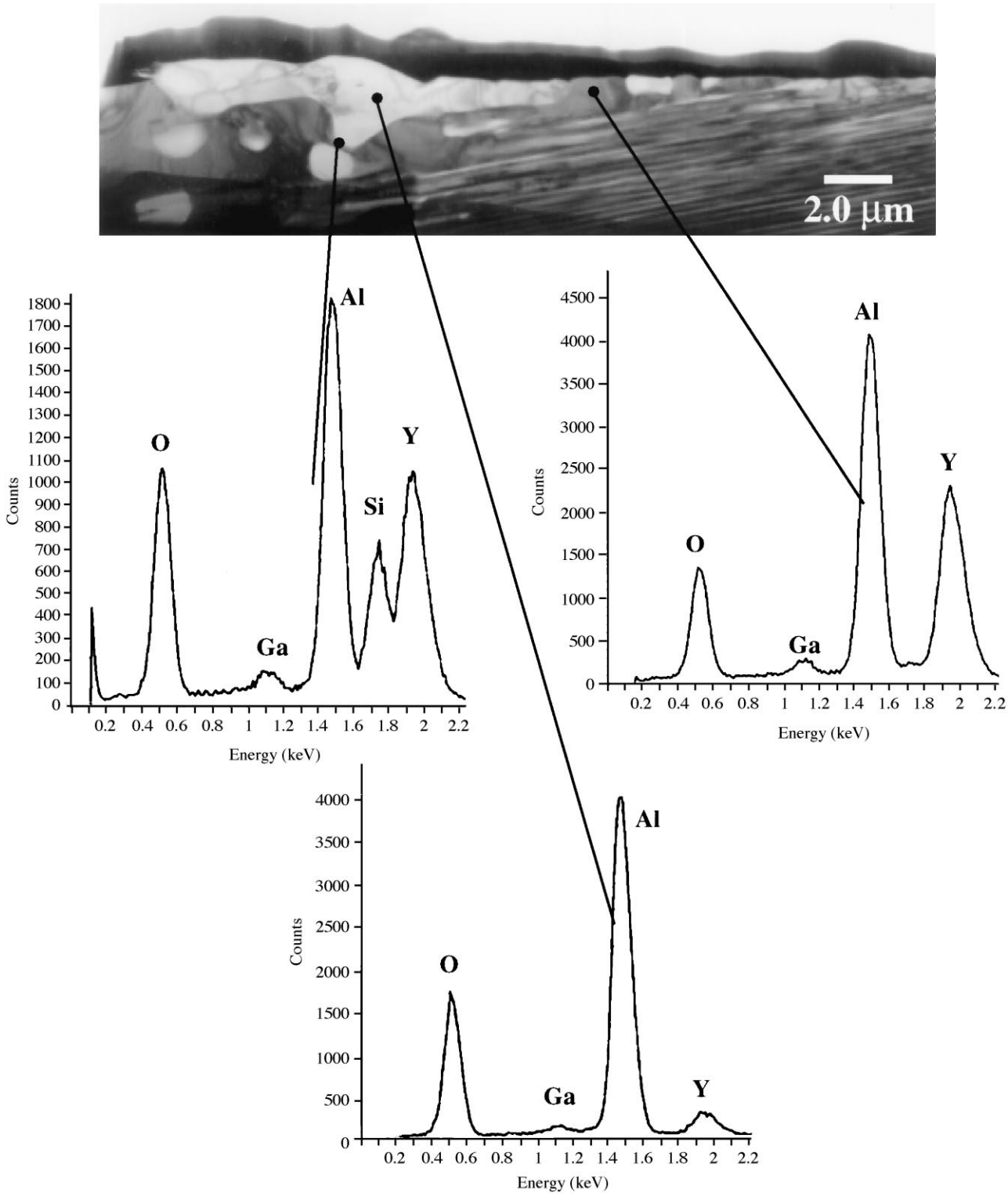

Figure 8. TEM micrograph and EDX spectra of the surface defect found in Fig. 3(d). This is a long term HT showing heterogeneous coarsening on AYE-SAP monofilament exposed for 50 h at 1400°C in air. The Ga signal results from the ion milling process.

It is important to point out that the classical rate theory analysis used by Yang implicitly assumes that $D \gg D_o$[59] by at least one order of magnitude (if not greater) and this may not be the case for Yang's data nor any data collected in this study. The maximum homogeneous coarsening factor of only 2·5 was observed. Similarly, the mechanism for rod coarsening was not discussed by Yang. One can visualize and model Ostwald ripening (coarsening without a morphology change) of a co-continuous microstructure through a ledge migration process which result in a time exponent less than 1/3. However, the extension of these arguments to a non-co-continuous situation like a rod microstructure is difficult. It will probably require rod branching and sphereodization (coarsening with a morphological change) to be present. Therefore, much longer annealing times are needed to validate the classical theory assumption and determine the mechanisms. These long term experiments are in progress. In any case, the slow homogeneous coarsening kinetics observed in the DS-AYE monofilament is much better than the ($t^{1/2}$) kinetics observed in grain growth in polycrystalline alumina fibers. Consequently, the strength retention should be very good and predictable from the phase size using Fig. 1. However, significant strength degradation has been reported after long term anneals.[32,38–41] This suggest the possibility of heterogeneous coarsening sites from the surface of the fiber becoming strength limited.

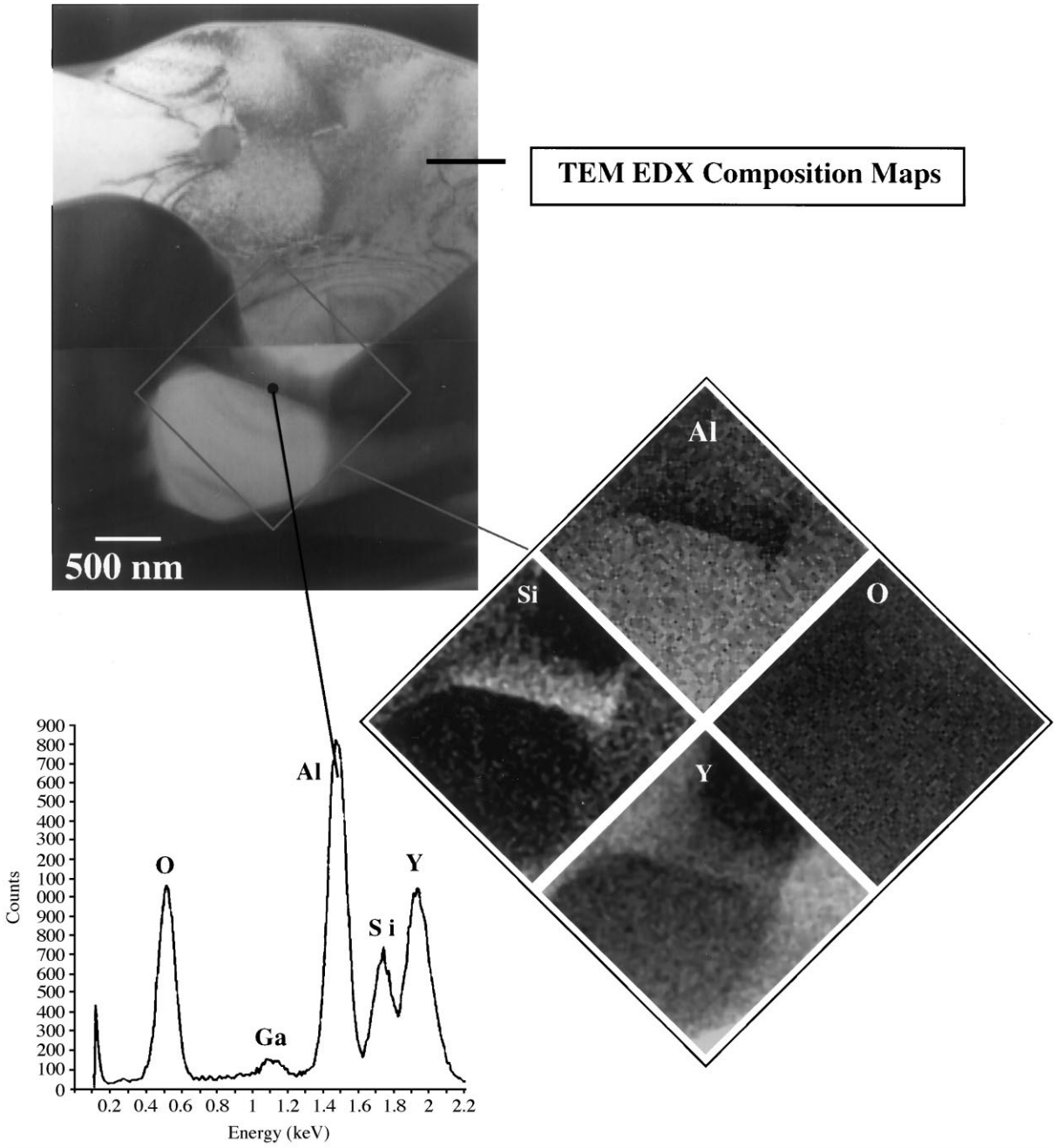

Figure 9. EDS mapping of TEM micrograph from the surface defect found in Figs 3(d) and 8. This is the long-term growth of heterogeneous coarsening on AYE-SAP monofilament exposed for 50 h at 1400°C in air.

3.2 Heterogeneous coarsening and strength retention

Heterogeneous or non-homogeneous coarsening has been observed in the AYE system by several investigators.[39–41]. These defects were observed in the SEM as the strength and rupture life limiting defects after high temperature anneals. This abnormal coarsening phenomenon appears as very large blotches on the fiber surface after long term anneals [Fig. 3(d)]. Chemical analysis of the fiber surface using SEM-EDX spectroscopy showed only Al, O, and Y present and in the same ratios as the unaffected microstructure. Hence, it was suggested that the eutectic system must have undergone discontinuous coarsening[54] similar to that found in some metal eutectic systems.[42,60] Additionally, it has been suggested that this type of instability may be inherent in all eutectic morphologies[38,61] and, therefore, limit their usefulness as high temperature materials. It is important to point out that the present theories on discontinuous coarsening are only valid for lamellar morphologies and not rod structures. However, in this study abnormal coarsening was also observed on fibers where the rod morphology had meandered to the fiber surface. [Fig. 3(d)] Additionally, in the systems where discontinuous coarsening has been observed substantial solid solubility existed and in this system it does not.

The results from in-depth SEM, EDX, and TEM analysis on these surface defects were used to rationalize the mechanism of heterogeneous coarsening. The analysis suggests that these defects are not a result of discontinuous coarsening but instead a result of a reaction of the fiber constituents with silica containing dust and dirt from handling and/or ambient air. A model has been constructed based on the present work to explain the sequence of events which have been observed in both short term and long term anneals (Fig. 4).

3.3 The model for heterogeneous coarsening

1. Silicates from dust and dirt land on the fiber and become liquid above 1300°C [Fig. 3(c)].
2. This liquid reacts rapidly with the YAG phase and decomposes it into a Yttrium Aluminum Silicate molten glass [Figs 3(c), 5–7] as predicted by the phase diagram.[62,63]
3. The alumina phase coarsens abnormally because diffusion is rapid in molten silicates and there is no crystallographic constraints at the glass/alumina interface. This continues until adjacent alumina phases impinge upon each other and form an alumina cap. TEM diffraction analysis shows the alumina in the cap contains the same OR as the original eutectic. The ingress of silicate into the monofilament causes the alumina grains to extrude from the surface in order to preserve a constant volume condition.
4. The entrapped silicate rapidly wets the interphase boundaries of the system, promoting coarsening of both alumina and the underlying YAG phase [Figs 3(d), 8 and 9].
5. After long term anneals, some of the silicate becomes trapped in the alumina/alumina boundaries and spheroidizes (Fig. 9). Silicon ions may go into solid solution in YAG as

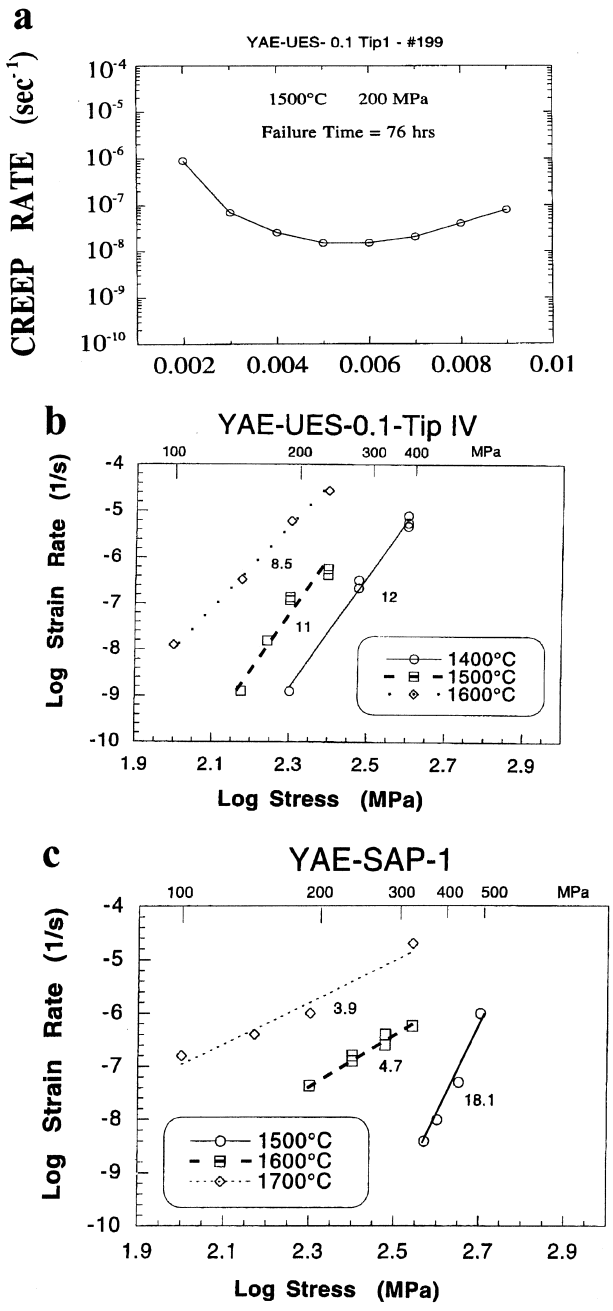

Fig. 10. Constant load tensile creep data. (a) Incremental strain rate versus strain data obtained from a single creep test. The minimum incremental strain rate regime is assumed to be at steady-state and its value is used in Fig. 10(b). (b) Logarithmic plots of the minimum creep strain rate versus the applied stress at various temperatures for the UES monofilament. (c) Logarithmic plots of the minimum creep strain rate versus the applied stress at various temperatures for the SAP monofilament.

long as some alkaline earth elements are also present.[64,65] This would tend to slow down or stop the rapid coarsening.

6. The shape difference of the defects that form on the monofilament surfaces with the Chinese script morphology (circular) versus the rod/plate eutectic (elliptical) can be accounted for by the anisotropy of the interphases themselves.

In summary, heterogeneous coarsening in the AYE monofilament appears to be the result of a reaction between the fiber constituents and silicates from dust and dirt. No evidence has been found suggesting discontinuous coarsening is occurring. The size of the defects which form will be a function of the scale of the starting DS microstructure, the size of the dust or dirt particle, the chemistry of the dust particle, the temperature, and the time of reaction. Kinetics of the reaction process is not extractable from this set of experiments, since the size of the contaminant and its chemistry were not controlled. It is important to realize that the high temperature mechanical properties that one has measured for this fiber may not be representative of its inherent high temperature mechanical properties, but rather an artifact of this reaction. It must be emphasized that heterogeneous coarsening should not be a 'show stopper' for this fiber system if good housekeeping practices are implemented prior to coating and incorporation into a matrix. All of which should tend to minimize or eliminate the occurrence of these defects.

3.4 Creep

The effects of heterogeneous defects also made the analysis for steady state creep difficult. Often rupture initiates at these sites while the fibers was still in the primary creep regime. In this study, a methodology was established in order to qualify the creep test results. First, only one test (constant load and temperature) was obtained per fiber so as not to complicate the interpretation. Constant load tensile creep data (displacement versus time) was then converted to incremental strain rate versus strain and plotted. Curves which passed through a minimum strain rate regime were assumed to be valid for steady-state creep analysis [Fig. 10(a)]; that is not affected by any heterogeneous coarsening defects in the gage section. Curves from tests which were stopped prior to reaching a minimum or failed during primary creep were not used in the steady state analysis which follows. However, fractography analysis on these prematurely failed samples did show that failure occurred at the heterogeneous defect site.

Logarithmic plots of the minimum creep rate versus the applied stress at various temperatures are shown in [Fig. 10(b) and (c)] for each monofilament. It is obvious from this data that the difference in microstructure between each fiber results in dramatic changes in creep behavior. TEM micrographs from selected crept samples showed high dislocation activity in the sapphire phase and moderate activity in the single crystal YAG phase [Fig. 11(a) and (b)]. Since dislocations were

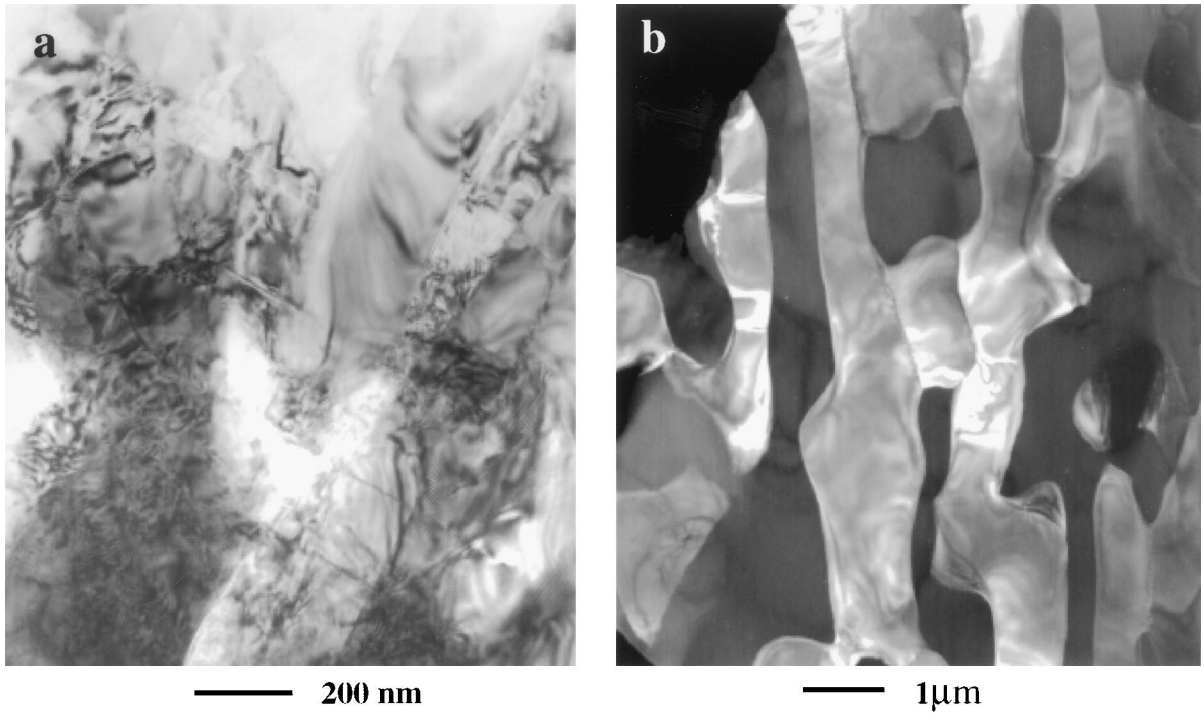

Fig. 11. TEM micrographs of tensile crept AYE monofilaments. (a) TEM bright field of AYE-SAP crept at 375 MPa at 1500°C showing high dislocation activity, shear bands, and twinning in the sapphire. (b) TEM-YAG dark field of AYE-UES crept at 125 MPa at 1500°C showing a recovered structure with dislocation networks forming low angle boundaries.

observed it is reasonable to consider a dislocation backstress argument to explain the high stress exponents (slope = n) observed in the logarithmic plots found in [Fig. 10(b) and (c)]. One possible source for this backstress is an Orowan pile-up and bowing mechanism[66,67] occurring in the sapphire matrix due to the presence of the more creep resistant single crystal YAG phase. The data from [Fig. 10 (b) and (c)] is replotted in Fig. 12(a) by including a threshold stress which was adjusted in order to get the effective stress exponent near a value of 5. The threshold stresses thus obtained are plotted versus temperature in Fig. 12(b). The plot shows that:

(a) the threshold stress converges for the two different microstructures at about 1650°C;
(b) the threshold stress goes to zero at about 1675°C (well below the eutectic melting point).

Figure 12(b) also includes a calculated barrier spacing (for both alumina and YAG) which corresponds to a selected threshold stress as predicted by the Orowan bowing stress formula:

$$\sigma_{\text{threshold}} = \alpha G b/\lambda$$

where α is the coherency factor = 0·5 for this system; G is the shear modulus; G_A at 1500°C = 133 GPa and G_Y at 1500°C = 110 GPa[14]; b is the Burgers vector; $b_A = 5{\cdot}12$ Å while $b_Y = 10{\cdot}4$ Å; λ is the barrier spacing or phase spacing.

This plot shows that:

(a) Good agreement exits when comparing observed YAG and alumina spacings found in each monofilament to the calculated barrier spacings required to produce a given threshold stress.
(b) According to the Orowan equation, a barrier spacing of around 4–6 μm would be required for the threshold stress to become negligable relative to the applied stress, thus providing no enhanced strengthening. This behavior has been observed in two separate studies on the compression creep on bulk DS-AYE where the transverse phase size was greater than 6 μm and the creep stress exponent maintained a value of 5 irrespective of the temperature.[23,68] [Fig. 12(c)].
(c) An average effective activation energy = 635 kJ/°K-mol can be calculated from the

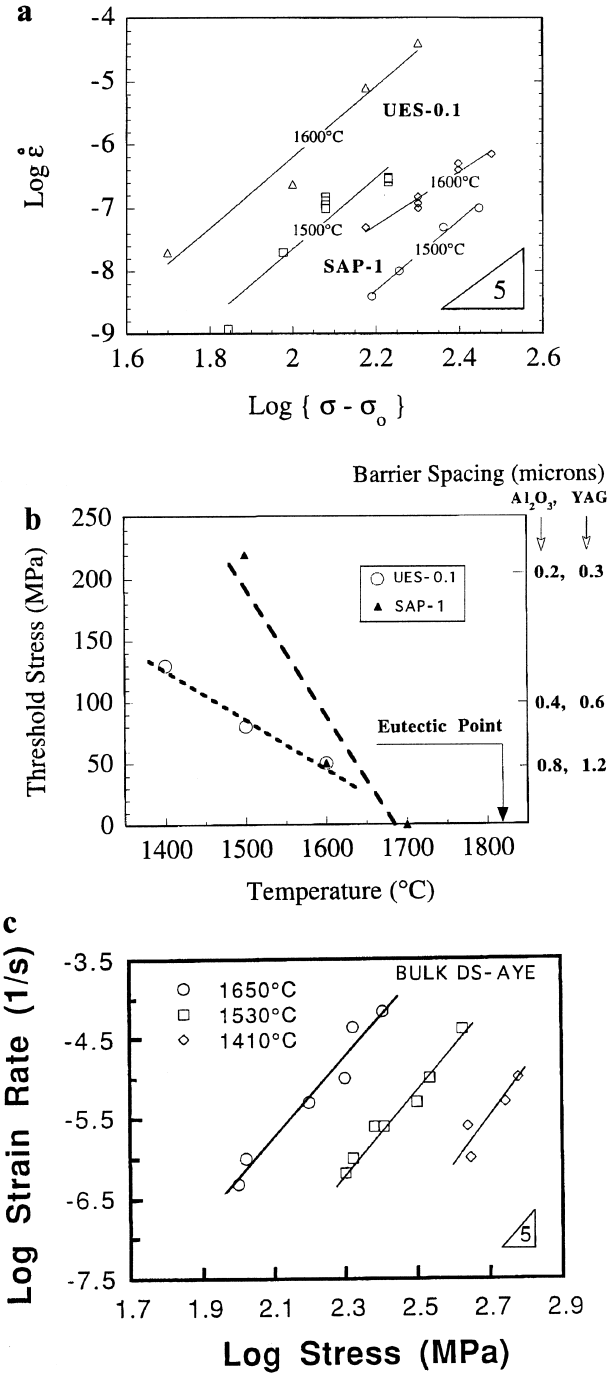

Fig. 12. Plots used in creep analysis. (a) Effective creep curves for both AYE-UES and the AYE-SAP data. An arbitary threshold stress is subtracted from the applied stress in [Fig. 10(b) and (c)] in order to get $n = 5$. (b) The threshold stresses used to create Fig. 12(a) are plotted versus temperature. (c) Compression creep data on bulk DS-AYE where the transverse phase size was greater than 6 micron and $n = 5$.[23]

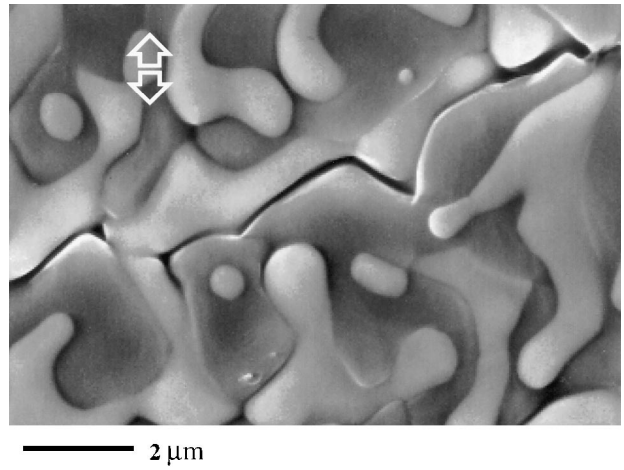

Fig. 13. SEM micrograph of AYE-UES sample crept in tension at 175 MPa and 1500°C showing rupture at the interphase boundary.

threshold stress adjusted creep plots in Fig. 12(a). This value compares well with the apparent activation energy of 650 kJ/°K-mol for compression creep of bulk DS-AYE where $n = 5$[23–68].

The steady-state creep behavior is eventually interrupted by cavitation at the interphase boundaries which did not lie parallel to the stress axis. At these interfaces dislocation pile ups, interact, and may become sessile. Relaxation of the stress by dislocation climb and glide is impaired and forces the strain to be accommodated by cavity development. In the third stage of creep, cavities start to grow and link up resulting in crack formation (Fig. 13). This eventually results in crack linkage and rupture of the monofilament.

4 Conclusion

Directionally solidified AYE monofilaments can be produced with various morphologies and microstructure scales depending upon the processing conditions. The RT tensile strength is predictable from the transverse phase size using a Hall–Petch type relationship. Homogenous coarsening is very slow and obeys a ($t^{1/4}$) kinetics consistent with an interface diffusion controlled mechanism. Heterogeneous coarsening is a result of surface reactions with silicon containing species from the environment and not a result of discontinuous coarsening observed in some metallic eutectic structures. Hot strength, annealed strength, and creep rupture of exposed fibers are limited by the extrinsic heterogeneous coarsening and not by the inherent homogenous coarsening. Heterogeneous coarsening should be eliminated or minimized by good housekeeping, coatings, and incorporation into a CMCs matrix. The steady-state creep behavior of the DS-AYE monofilament is a strong function of the microstructure scale, morphology, and aspect ratio. Enhanced creep strength can be obtained with fine, aligned phases due to the development of a substantial dislocation backstress. Creep resistance approaches that of single crystal YAG and is superior to sapphire. Rupture occurs by the linkage of cavities formed at the interphase boundaries during the ternary creep stage. The scientific merit of this research lies in the fact that fine, interpenetrating, aligned, single crystal structures can provide both high tensile strength as well as superior creep resistance. The DS-AYE monofilament should be an excellent choice for a fiber to meet the ultra high temperature, long life component designs for oxidizing environments. Additionally, many metallurgical processes produce similar type-microstructures and many emerging technologies could benefit from such engineered materials.

Acknowledgements

We would like to thank the following people for their assistance, patience and insight: (a) T. Mah (UES), D. Petry (UES) and J. Collins (Saphikon) for the AYE monofilaments. (b) R. Wheeler (UES), F. Scheltens (UES) and S. Farmer (NASA LeRC) for assistance in TEM operation and analysis. (c) D. Via (WSU, OH) for assistance in the operation of the focused ion beam FIB. (d) J. Yang (UCLA) and A. Ardel (UCLA) for helpful discussions and data on coarsening. (e) T. A. Parthasarathy (UES) and A. Sayir (NASA LeRC/CWRU, OH) for helpful discussions on mechanical properties and creep analysis. (f) C. Crooks (UES) for assistance with preparing the manuscript.

References

1. Courtright, E. L., Engineering property limitations of structural ceramics and ceramic composites above 1600°C. *Cer. Eng. Sci. Proc.*, 1993, **12**, 1725–1744.
2. Courtright, E. L. *et al.*, *Ultra High Temperature Composite Assessment Study*. USAF-AFWAL-TR-91-4061., Battelle NW Labs, Richland Washington, 1991.
3. DiCarlo, J. A. *et al.*, *Current issues for SiC and oxide fiber development*. HITEMP Review, NASA Conf Pub 10051, Cleveland, OH, 1990.
4. DiCarlo, J. A. *et al.*, *High temperature structural fibers—status and needs*. NASA Technical Memorandum 105174. Cleveland OH.1991.
5. DiCarlo, J. A., Creep limitations of current polycrystalline ceramic fibers. *Comp. Sci. Technol.*, 1994, **51**, 213–222.
6. Wilson, D. M., Lunenburg, D. C. and Lieder, S. L., High temperature properties of Nextel 610 and alumina-based nanocomposite fibers. *Cer. Eng. Sci. Proc.*, 1993, **14**(7–8), 609–621.
7. Wilson, D. M., Lieder, S. L. and Luenenburg, D. C., Microstructure and high temperature properties of Nextel 720 fibers. *Ceram. Eng. Sci. Proc.*, 1995, **16**(5), 1005–1014.
8. Firestone, R. F. and Heuer, A. H., Creep deformation of zero degree sapphire. *J. Am. Ceram. Soc.*, 1976, **59**(1–2), 24–29.
9. Jones, L. E. and Tressler, R., The high temperature creep behavior of oxides and oxide fibers. NASA CR-187060, Cleveland OH, 1991.
10. Collins, J. M., Bates, H. E. and Fitzgibbon, J. J., Growth and characterization of single crystal YAG fibers. USAF-WL-TR-4083, 1994, Saphikon Inc., Nashua NH.
11. Sheehan, J. E., Mechanical properties of $MgAl_2O_4$ single crystal fibers. *SDIO Newsletter*, 1993, **10**, 5–11.
12. Sheehan, J. E., Sigalovsky, J. and Haggerty, J. S., Mechanical properties of $MgAl_2O_4$ single crystals. In *Proceedings of the 17th Annual Conference on Composites and Advanced Ceramics*. Cocoa Beach FL, 1992..
13. Sheehan, J. E. and Haggerty, J. S., Single crystal magnesium aluminum spinel fibers. DOD-Battelle Pacific NW Labs-#036954-A-F1, 1993, MSNW Inc.
14. Corman, G. S., *Creep of Oxide Single Crystals*. USAF-WRDC-TR-90-4059, 1990, General Electric Corp.

15. Corman, G. S., High temperature creep of some single crystal oxides. *Ceramic Engineering and Science Proceedings*, 1991, **12**(9-10), 1745–1767.
16. Sayir, A., Time dependent strength of sapphire fibers at high temperatures. In *Advances in Ceramic Matrix Composites I*, ed. N. Bansal. Am. Ceram. Soc., Westerville, OH, pp. 691–702.
17. Wiederhorn, S. M., Hockey, B. J. and Roberts, D. E., Effects of temperature on the fracture of sapphire. *Phil. Mag*., 1973, **28**, 783–796.
18. Crane, R. L., An investigation of the mechanical properties of silicon carbide and sapphire filaments. USAF-AFML-TR-72-180, 1972.
19. Crane, R. L. and Tressler, R. E., Effects of surface damage on the strength of C-axis sapphire filaments. *J. Comp. Mat*., 1971, **5**, 537–541.
20. Pysher, D. J., Strengths of ceramic fibers at elevated temperatures. *J. Am. Ceram. Soc*., 1989, **72**(2), 284–288.
21. Tressler, R. E. and Barber, D. J., Yielding and flow of sapphire fibers. *J. Am. Ceram. Soc*., 1974, **57**(1), 13–19.
22. Parthasarathy, T. A., Mah, T. and Matson, L. E., Creep behavior of an Al_2O_3–$Y_3Al_5O_{12}$ eutectic composite. *Ceram. Eng. Sci. Proc*., 1990, **11**(9–10), 1628–1638.
23. Parthasarathy, T. A., Mah, T. and Matson, L. E., Deformation behavior of an Al_2O_3–$Y_3Al_5O_{12}$ eutectic composite in comparison with sapphire and YAG. *J. Am. Ceram. Soc*., 1993, **76**(1), 29–32.
24. Courtright, E. and Haggerty, J. S., Controlling microstructures in $Zr_2O(Y_2O_3)$–Al_2O_3 eutectic fibers. *Ceram. Eng. Sci. Proc*., 1993, **14**(7–8), 671.
25. Mah, T. *et al*., Directionally solidification of refractory oxide ceramic eutectic composites. USAF-WRDC-TR-90-4081, 1990
26. Mah, T. and Matson, L. E. *et al*., Fabrication of alumina–Yttriun aluminum garnet (YAG) eutectic fibers. USAF Invention Disclosure #19666, 1990.
27. Mah, T. *et al*., Feasibility study of refractory oxide eutectic fiber production. USAF-SBIR-Phase 1, #F33615-90-C-5934, 1991, UES Inc., Dayton, OH.
28. Mah, T., Processing, microstructure and properties of alumina-YAG eutectic fibers. *Ceram. Eng. Sci. Proc*., 1993, **14**(7–8), 622–638.
29. Mah, T., Processing, microstructure and properties of Al_2O_3-$Y_3Al_5O_{12}$ (YAG) eutectic fibers. *SDIO Newsletter*, 1993, **10**, 21–23.
30. Collins, J. M., Yang, J. and Sayir, A., 75 micron YAG–alumina eutectic fiber. AFOSR-Phase 2-SBIR; #F49620-96-C-0047, 1998, Saphikon Inc.
31. Sayir, A. and Matson, L. E., Strength of AYE fibers made by LHFZ. NASA LeRC advance high temperature engine materials technology program. In *Proc. of the 3rd Annual HITEMP Review*. 1991, Cleveland, OH.
32. Sayir, A. and Matson, L. E., Growth and characterization of directionally solidified $Al_2O_3/Y_3Al_5O_{12}$ (YAG) eutectic fibers. In *Proceedings of the 4th Annual HITEMP Review: Advanced High Temperature Engine Materials Technology Program*. NASA CP10082. 1992, NASA: NASA LeRC. pp. 83–1 to 83–13.
33. Sayir, A. and Matson, L. E., Directionally solidified $Al_2O_3/Y_3Al_5O_{12}$ (YAG) eutectic fibers. In *15th Conference on Metal Matrix, Carbon and Ceramic Matrix Composites*, Cocoa Beach Fl., 1991.
34. Mah, T. *et al*., Development of continuous refractory oxide eutectic fibers., USAF-WPAFB-Phase 2-SBIR, #F33615-91-C-5655, WL-TR-94-4087, UES Inc., 1994.
35. Collins, J., 75 micron YAG–alumina eutectic fiber. AFOSR-Phase 1-SBIR, #F49620-95-C-0065, Saphikon Inc., 1996.
36. Chalmers, B., Labelle, H. E. and Mlavsky, A. I., Edge-defined, film-fed growth. *J. Crystal Growth*, 1972, **13/14**, 84–87.
37. Regester, R. F., Ph.D. thesis, University of Pennsylvania, 1963.
38. Sayir, A., Farmer, S. C. and Dickerson, P. O., Status of single crystal and directionally solidified oxide fibers. NASA LeRC Tech. Brief, 1996.
39. Sayir, A. *et al*., High temperature mechanical properties of directionally solidified $Al_2O_3/Y_3Al_5O_{12}$ (YAG) eutectic fibers. In *HITEMP Review 1994: Advanced High Temperature Engine Materials Technology Program*. NASA CP10082. 1994.
40. Farmer, S. C. *et al*., Microstructural stability and strength retention in directionally solidified Al_2O_3–YAG eutectic fibers. In *20th Annual Conference on Composites and Advanced Ceramics*. CoCoa Beach Fl, 1995.
41. Yang, J. M., Jeng, S. M. and Chang, S., Fracture behavior of directionally solidified $Y_3Al_5O_{12}/Al_2O_3$ eutectic fiber. *J. Am. Ceram. Soc*., 1996, **79**(5), 1218–1222.
42. Livingston, J. D. and Cahn, J. W., Discontinuous coarsening of aligned eutectic. *Acta Metall*., 1974, **22**, 495–503.
43. Ardell, A. J., Coarsening of directionally-solidified eutectic microstructures. In *Proceedings of the Conference on Computer-Aided Design of High Temperature Materials*. Santa Fe, NM, July 1997.
44. Caslavsky, J. L. and Viechnicki, D. J., Melting behaviour and metastability of yttrium aluminium garnet (YAG) and $YAlO_3$ determined by optical differential thermal analysis. *J. Mat. Sci*., 1980, **15**, 1709–1718.
45. Caslavsky, J. L. and Viechnicki, D. J., Melting behavior and metastability of yttrium aluminum garnet (YAG) and $YAlO_3$ determined by optical differential thermal analysis. *J. Am. Ceram. Soc*., 1980, **15**, 1709.
46. Viechnicki, D. and Schmid, F., Investigation of the eutectic point in the system Al_2O_3-$Y_3Al_5O_{12}$. *Mat. Res. Bull*., 1969, **4**, 129–136.
47. Matson, L. E., Hay, R. S. and Mah, T., Stability of a sapphire-yttrium aluminum garnet composite system. *Ceram. Eng. Sci. Proc*., 1989, **10**, 764.
48. Mah, T., Parthasarathy, T. A. and Matson, L. E., Processing and mechanical properties of $Al_2O_3/Y_3Al_5O_{12}$ (YAG) eutectic composites. *Ceram. Eng. Sci. Proc*., 1990, **11** (9–10), 1617–1627.
49. Mah, T. and Petry, M. D., Eutectic composition in the pseudobinary of $Y_4Al_2O_9$ and Y_2O_3. *J. Am. Ceram. Soc*., 1992, **75**(7), 2006–2009.
50. LaBelle, H. E. and Miavsky, A. I., Growth of controlled profile crystals from the melt: Part 1—sapphire filaments. *Mater. Res. Bull*., 1971, 6, 571.
51. Haggerty, J. S., Wills, K. C. and Sheehan, J. E., growth and properties of single crystal oxide fibers. *Ceram. Eng. Sci. Proc*., 1991, **12**(9–10), 1785–1801.
52. Sigalovsky, J., Growth characteristics, and properties of spinel single crystal fibers. *Ceram. Eng. Sci. Proc*., 1992, **13**(7–8), 183–189.
53. Sheehan, J. E., Mechanical properties of single crystal oxide fibers. In *DoD/CIAC Workshop on Ceramic Matrix Composites*. 1991, Alexandria, Virginia.
54. Yang, J. M., UCLA, personal communication, 1996.
55. Ardell, A. J., On the coarsening of grain boundary precipitates. *Acta Metall*., 1972, **20**, 601.
56. Haneda, H., Miyazawa, Y. and Shirasaki, S., Oxygen diffusion in single crystal yttrium aluminum garnet. *J. Cryst. Growth*, 1984, **68**, 581–588.
57. Parthasarathy, T. A., Mah, T. and Keller, K., Creep mechanism of polycrystalline yttrium aluminum garnet. *J. Am. Ceram. Soc*., 1992, **75**(7), 1756–1759.
58. Hay, R. S., Kinetics and deformation during the reaction of yttrium–aluminum perovskite and alumina to yttrium–aluminum garnet. *J. Am. Ceram. Soc*., 1994, **77**(6), 1473–1485.
59. Ardell, A. J., *Phys. Rev. Lett*., 1995, **74**, 4960.
60. Martin, J. W. and Doherty, R. D., Stability of microstructure in metallic systems. In *Cambridge Solid State Science Series*, ed. R. W. Cahn. Cambridge: University Press, Cambridge, 1976, 298.
61. Bates, H. E., EFG growth of alumina-zirconia eutectic fiber. In *Proceedings of the 16th Conference on Composites and Advanced Ceramics*. Cocoa Beach Fl., 1992.
62. Levin, E. M., Robbins, C. R. and McMurdie, H. F., *Phase Diagrams for Ceramics 1969 Supplement*, ed. M. K. Reser. The American Ceramic Society, 1969, pp. 165, Fig. 2586.

63. Mah, T. and Parthasarathy, T. A., Effects of temperature, environment and orientation on the fracture toughness of single crystal YAG. *J. Amer Ceram. Soc*., 1997, **80**(10), 2730–2734.
64. Keith, M. L. and Roy, R., *Am. Min*., 1954, **39**, 1.
65. Aasland, S. and McMillan, P. F., Density-driven liquid–liquid phase separation in the Al_2O_3-Y_2O_3 system. *Nature*, 1994, **369**, 633.
66. Strudel, J. L., Mechanical properties of multiphase alloys. In *Physical Metallurgy*, ed. R. W. Cahn and P. Haasen. Elsevier Science Pub, Amsterdam, 1983, 1481.
67. Legzdina, D. and Parthasarathy, T. A., Deformation mechanisms of a rapidly solidified Al-8.8Fe-3.7Ce alloy. *Metallurgical Transactions A*, 1987, **18A**, 1713–1719.
68. Waku, Y., Nakagawa, N. and Kohtoku, Y., The creep and thermal stability characteristics of a unidirectionally solidified Al_2O_3/YAG eutectic composite. *J. Mat. Sci*., 1998, **33**(20), 4943.